Ultrahigh vacuum instrument that combines variable-temperature scanning tunneling microscopy with Fourier transform infrared reflection-absorption spectroscopy for studies of chemical reactions at surfaces

David Beck, Matthias Batzill, Christof Baur,[a] Jooho Kim, and Bruce E. Koel[b]
University of Southern California, Los Angeles, California 90089-0482

(Received 1 August 2001; accepted for publication 29 November 2001)

We describe the construction of an ultrahigh vacuum chamber that incorporates variable-temperature scanning tunneling microscopy (STM), Fourier transform infrared reflection-absorption spectroscopy (FT-IRAS), Auger electron spectroscopy, low-energy electron diffraction, and temperature programmed desorption, for studying structure and reactivity at surfaces. The chamber and manipulator design enables *in situ* sample preparation and analysis, and rapid access to several surface-analytical techniques by rotation only. This eliminates sample inconsistencies due to *ex situ* preparation or the necessity to run parallel experiments. Inclusion of FT-IRAS allows us to characterize surface species and identify adsorbates during studies using STM. © *2002 American Institute of Physics.* [DOI: 10.1063/1.1445863]

I. INTRODUCTION

Scanning tunneling microscopy (STM)[1,2] is one of the most powerful tools in use today for studying the surface structure of conducting and semiconducting samples. The great strength of this technique lies in its ability to resolve atomic-size features in ''real space.'' This enables one to probe local surface morphology without the spatial averaging restrictions common to other surface structure probes. With recent advances in the theory and technology of STM, molecular identification, manipulation, and most recently, the initiation of individual chemical events have been realized.[3,4]

As surface scientists, we are keenly interested in understanding the relationship between structure and reactivity at surfaces. For example, we have characterized changes in the chemical behavior of binary surface alloys due to changes in composition and two-dimensional order using various structural[5–7] and chemical[8–10] probes, but ultimately have been hindered by an incomplete knowledge of the local morphology of the surface. In order to accurately ascribe structure-property relationships, the local surface structure must be identified. STM is useful in this regard, and in addition, STM enables us to observe steps, defects, domain boundaries, and other inhomogeneities that may also be relevant to elementary reaction steps.

Vibrational information from Fourier transform infrared spectroscopy (FTIR) is a powerful tool for identifying molecular fragments and stable molecules at surfaces. Several groups have used STM and FTIR in parallel experiments in vacuum[11–13] and in solution.[14] The inclusion of STM and FTIR into a single chamber allows important aspects of surface chemistry to be probed, which were difficult to address in years past. Experiments can be performed on a single sample under identical conditions, thus eliminating many inconsistencies. Adsorbate identity and geometry can be determined by using FTIR, and surface structures, even adsorption sites, can be assigned by using STM. This powerful combination of techniques allows us to investigate the relationship between surface structure and reactivity with atomic level detail and control.

II. INSTRUMENT DESIGN

A. The UHV system

The chamber design was based on two instruments built in Comsa's group.[15,16] The entire system is built with STM in mind and focuses on vibration minimization and easy *in situ* sample access to each of the different techniques. We have addressed the first of these objectives at two distinct levels of engineering: (i) the chamber beam-frame and support assembly and (ii) the sample holder/manipulator.

A photograph of the ultrahigh vacuum (UHV) system is shown in Fig. 1. The chamber is firmly bolted, using 1-in.-sq steel tubing and welded struts, to a wooden beam frame made of laminated 1×12 in. red oak boards. This material was chosen because of its vibrational damping characteristics and relative ease of construction.[17] The two primary beams are 55-in.-long and have 1/8-in.-thick lead sheets between each adjacent pair of four boards. The lead adds additional vibrational damping and weight to the structure. Five 39-in.-long cross-beams were constructed with four, laminated 1×6 in. boards to provide the support to which the chamber is attached. The beam frame sits on four Newport I-2000 High Performance Laminar Flow Isolators (air legs) to minimize vibrational coupling between the beam-frame and the floor. This system sits on an 8-ft thick slab of concrete on the ground floor of a building to provide it with a stable foundation.

By restricting sample motion to a single plane, we were able to use a compact, rigid manipulator which satisfied both primary objectives. This allows the sample to be positioned

[a]Present address: Zyvex, 1321 North Plano Road, Richardson, TX 75081.
[b]Author to whom correspondence should be addressed; electronic mail: koel@chem1.usc.edu

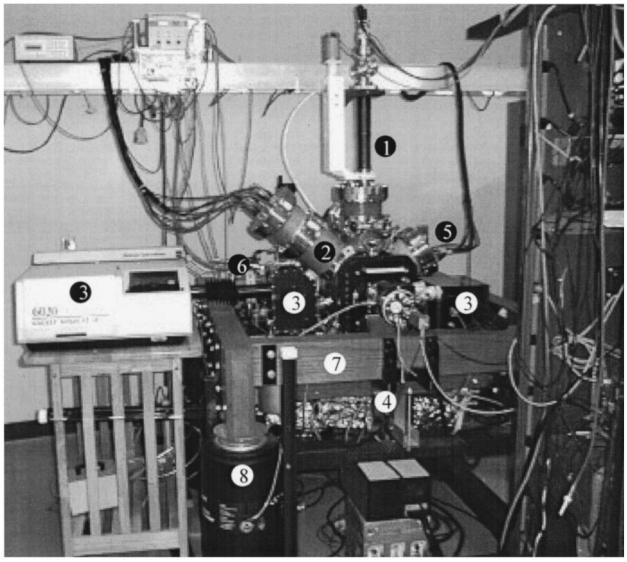

FIG. 1. Photograph of the UHV-STM chamber. (1) STM transfer-rod bellows, (2) CMA, (3) FT-IRAS mirror and detector purge boxes, (4) QMS, (5) LEED optics, (6) cryostat cold finger, (7) wooden beam frame, and (8) laminar flow air legs.

for different techniques by rotational only, while enabling minor "x/y" adjustments needed for optimization. Figure 2 shows a cross section of the chamber across the instrumental plane including the various techniques as they are situated around the sample. Current instrumentation includes a custom STM head connected to an RHK 1000 controller,

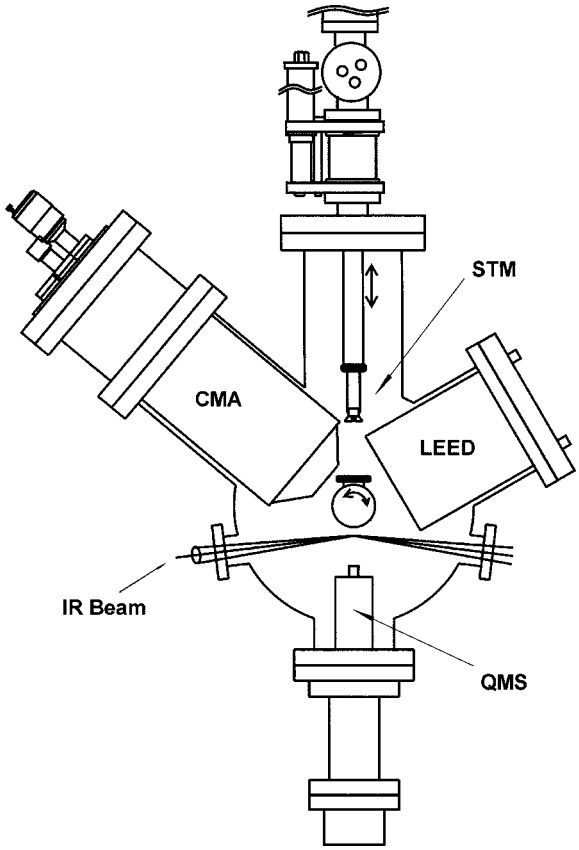

FIG. 2. Cross section of the chamber in the surface analysis plane showing the instrumentation.

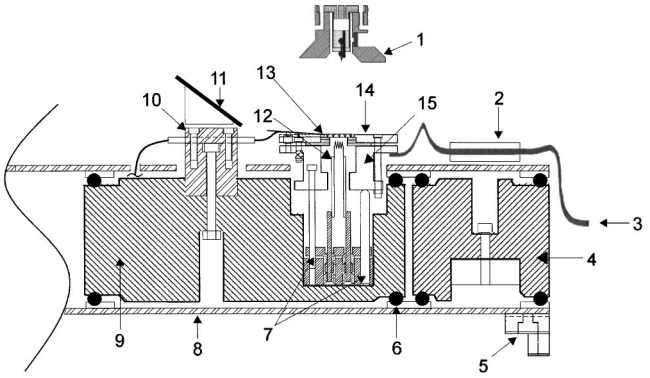

FIG. 3. Cross section of the sample holder: (1) STM, (2) copper-braid clamp, (3) copper braid, (4) secondary copper block, (5) support feet, (6) O-ring elastomer vibration isolators, (7) pushing-and-pulling screws, (8) stainless-steel support tube, (9) primary copper block, (10) clamp for thermocouple and tunneling-current wires, (11) mirror for monitoring tip position during course approach, (12) filament, (13) sample and three supporting sapphire disks, (14) upper Mo section, and (15) lower Mo block.

double-pass CMA (Perkin Elmer 11-055) for Auger electron spectroscopy (AES), ultraviolet photoelectron spectroscopy, and x-ray photoelectron spectroscopy, Fourier transform infrared reflection-absorption (FT-IRAS) optics and instrumentation (Mattson model 6020), quadrupole mass spectrometer (QMS) (UTI 100C) used for residual gas analysis and temperature programmed desorption (TPD), and reverse-view low-energy electron diffraction (LEED) optics (PRI RVL-120).

Directed toward the sample from out-of-plane positions are also an ion gun (Perkin Elmer 20-045) for sample cleaning, several resistively heated, metal evaporators for metal (e.g., Sn, Ag, and Ge) deposition, and precision leak valves (Varian 951-5106) for gas dosing. The system is pumped by two 220-l/s ion pumps (Perkin Elmer), which can be isolated by an 8 in. gate valve, and a turbomolecular pump (Pfeiffer TMU260) backed by a two-stage mechanical pump (Alcatel). The system has a typical base pressure of 2×10^{-10} Torr following bakeout. It is necessary to turn off the turbomolecular and mechanical pumps during imaging with the STM, and so vacuum ballast is employed for continuous pumping of the differentially pumped seal in the manipulator.

B. Sample holder

The sample holder was adapted from a design used by Comsa's group.[15,16] It must provide vibration isolation and allow for heating, cooling, and positioning of the sample. As shown in Fig. 3, the entire assembly consists of four main parts: molybdenum sample holder, primary copper block, secondary copper block (braid clamp), and stainless-steel tube.

The molybdenum sample holder is made of two parts. The lower portion is firmly fixed to the primary copper block by pushing-and-pulling screws. Two Ta rods extend through a cavity in the center of the Mo sample holder and attach to a 0.25-mm thoriated tungsten filament that is used to heat the sample radiatively or by electron bombardment. A large sapphire disk (23.75×1 mm) and two smaller ones (12×1 mm), each with a 6.4-mm hole in the center, sit on top of the lower Mo piece. The sample sits on top of these and is held in place

by three tungsten leaf springs. These provide resilient mechanical contacts and resist deformation due to extensive temperature cycling, and are held in place by electrically isolated Ta screws. The upper Mo piece presses down on the sapphire disks and is held firmly in place with Mo screws. It also provides a flat surface for the STM to sit on while scanning. A chromel–alumel (Type K) thermocouple is spot-welded directly to the side of the sample to measure the temperature. A Kapton™-shielded wire is attached to one of the tungsten leaf-spring sample clamps to enable measurement of the tunneling current during STM and allow for biasing the sample. It is held rigidly, close to the sample, in a wire clamp (No. 10, Fig. 3) which also acts as a heat sink to minimize heating of the wire. The thermocouple is also captured by this wire clamp. Ceramic tubing isolates the thermocouple over the length of the manipulator. A copper braid is clamped to the underside of the lower Mo block to form a thermal bridge to the cryostat and allow for sample cooling.

The primary copper block is designed to provide inertial dampening for the Mo sample holder. Six stainless-steel pushing-and-pulling screws (three pushing and three pulling) rigidly fix the Mo sample holder to the copper block and thermally isolate it from the copper block since stainless steel conducts heat poorly at low temperatures. The purpose of the second copper block is to provide a mechanically isolated clamping point for the copper braid midway between the sample holder and the ''cold finger'' to reduce vibrations that arise from boiling cryogen.

The copper blocks are held in place within the stainless-steel tube by Viton™ O-rings. These O-rings are press-fit into complimentary grooves in the copper blocks and circular stainless-steel clamps that fit snugly inside the outer tube. These clamps, and thus the entire assembly, are fixed in place with screws that extend through the stainless-steel tube into tapped holes in the clamps. The O-rings serve to isolate the copper blocks both electrically and vibrationally from the stainless-steel tube.

When the sample is positioned for STM imaging, the entire manipulator assembly is lowered so that ''feet'' attached to the bottom front of the tube come to rest on a tripod that is bolted to the bottom of the chamber. This setup holds the outer tube rigidly during scanning with the STM.

C. Cooling

The sample is cooled using a Janis ST-400 UHV Supertran™ cryostat with temperature controller. Using liquid nitrogen, we have cooled the sample to 138 K, but we expect to reach 100 K with minor modifications. For future experiments, we plan to use liquid helium to achieve temperatures of 50–60 K. The cold finger is mounted on a 2.75 in. flange and extends 7.5 in. in to the chamber through a stainless-steel support tube. The end of the cold finger protrudes 0.75 in. from the end of the tube, allowing easy access for attaching a copper braid. The cold finger is rigidly held by two sets of eight set-screws that extend through the tube and make point contact with the body of the cold finger. This setup provides stability for the cold finger and reduces vibrations of the rod. The use of a copper braid as the thermal conduit between the sample holder and cold finger is a method used previously by several groups, and we have made only minor modifications in our design.[15,18] Such a copper-braid capturing/decoupling device (Fig. 3 Nos. 2–4) between the cold finger and the sample holder attachment point has also been used previously and was shown to be effective.[16]

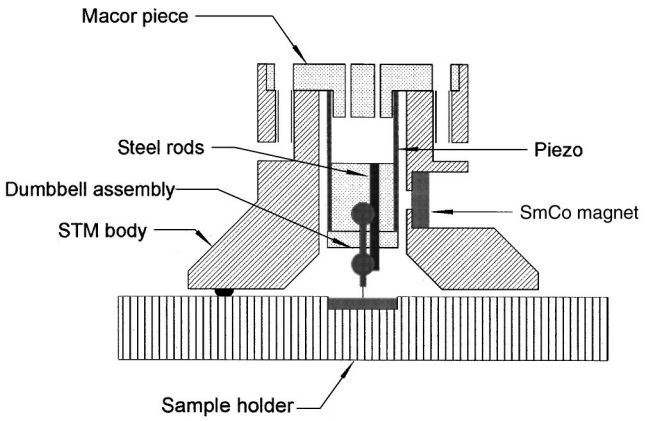

FIG. 4. Cross section of STM head. The dumbbell and tip assembly is held against the rods by a SmCo magnet. Course approach is accomplished by application of a cycloid voltage waveform to the *z* component of the piezo.

D. STM design

The STM, which is a stand-alone version of a design by Mugele *et al.*,[19,20] was constructed using a single-piezo tube design that utilizes a segmented, nickel-plated EBL No. 2 piezo (Staveley Sensors Inc.) for coarse, as well as fine positioning. Figure 4 shows a schematic of this STM. One advantage of this design over a ''beetle'' with several legs, is that the compact structure of this design provides increased immunity to vibrations and improves reliability because of the significantly reduced number of electrode wires. Another significant advantage is that this design avoids the common problems encountered from changes in the surface of the attendant ramp used for coarse approach that are caused by deposition and gas exposures in the STM experiments. The piezo is glued using Torr-Seal™ onto a Macor™ disk that fits snuggly into the top of the STM body and through which wiring extensions are inserted. Two stainless-steel rods are glued in place inside the piezo to form the tracks for translation of the tip holder. The tip is inserted into a ferromagnetic ''dumbbell'' assembly that is pulled against the tracks by a SmCo magnet. This dumbbell is held in place vertically by friction forces. Coarse approach of the tip is accomplished using a slip-stick mechanism whereby the tip assembly is ''shaken'' up or down by applying an appropriate cycloid voltage waveform to the *z* component of the piezo.[19,20] This design is very reliable and can be performed repeatedly without crashing the tip into the sample.

The STM is lowered onto the Mo sample holder from above using a linear motion drive as shown in Fig. 2. It is mounted at the end of a long transfer rod that allows us to position the STM head for scanning, tip exchange, and complete retraction during bakeout. The entire rod assembly consists of two sections. An upper transfer rod with ceramic tubing running down the outside for the STM wiring coming

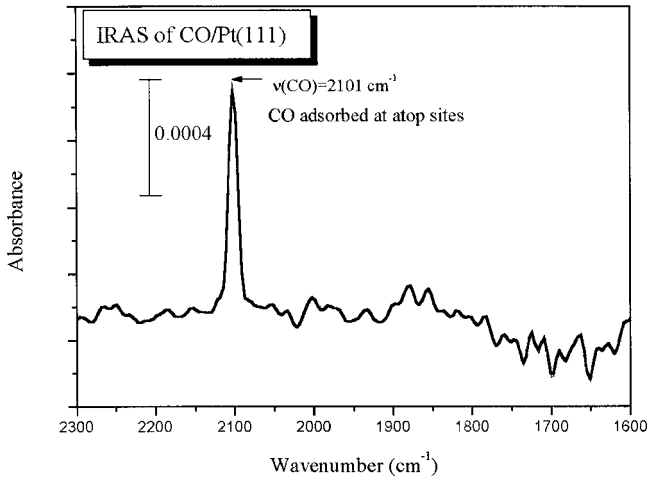

FIG. 5. FT-IRAS spectra of CO adsorbed on clean Pt(111).

from the pin connector feedthrough, and a lower section made of two 5-in. half-cylinders through which thin gold wiring extensions are routed and to which the STM is attached. A metal collar and Viton™ O-ring at the end of the upper section are designed to be ''captured'' by a support rigidly attached to the inside of the chamber in order to prevent the rod from shaking during scanning. In this position, the stainless-steel transfer bellows are fully compressed to further reduce vibrations. Below the collar, a 5-in. hollow cylinder (two halves) is attached that serves to protect the gold wiring (0.002 in.) and hold the STM. Two pins extend out from the top of the STM head through slots in the end of the hollow cylinder. When the STM head ''lands'' on the sample holder, the pins are moved out of contact with the cylinder by lowering the entire rod 1–2 mm further. This design ensures that the STM will be mechanically and electrically decoupled from the rod assembly in the scanning position. The STM contacts the sample holder via three 0.05-in. stainless-steel balls that are press-fitted into holes in the bottom of the STM body to minimize contact with the Mo sample holder surface. This allows the STM body to be maintained at moderate temperatures during sample cooling.

E. FT-IRAS

A Mattson 6020 FTIR is operated in a remote-detection mode for IRAS measurements. CaF_2 windows are located on the chamber in the plane of rotation of the sample such that the incident/reflected angle of the IR beam is 7° with respect to the sample surface plane.

The mirror and external detector boxes used in FT-IRAS are firmly attached to the beam frame. Because the mirror boxes must be purged continuously using H_2O- and CO_2-free air for several hours prior to an experiment, beam path optimization must be performed prior to initiating an experiment. A MCT narrow band detector is used because of its high signal-to-noise over the operating bandwidth.

A FT-IRAS spectrum following a saturation dose of CO on Pt(111) at 300 K is shown in Fig. 5.

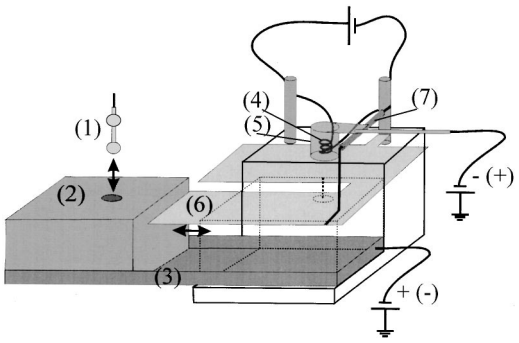

FIG. 6. STM-tip heater and sputtering device: (1) STM tip and dumbbell, (2) molybdenum block, (3) stainless-steel tray, (4) filament, (5) tantalum cylindrical shield, (6) stainless-steel foil shield, and (7) ceramic tube.

F. *In situ* STM-tip transfer and cleaning

Rigorous cleaning in vacuum of electrochemically etched, tungsten STM tips, is necessary to remove the tungsten oxide film, which coats the tip in order to improve the tunneling characteristics. Many different approaches have been discussed in the literature, but most of them involve high-temperature annealing[21–24] and/or ion sputtering.[23–27] Sharpening of single crystal tips has been demonstrated using ion bombardment from behind the tip[25,26] as well as for ''head-on'' ion bombardment.[24–27] For polycrystalline tips, prolonged sputtering can result in a degradation of the shape of the tip due to preferential sputtering at grain boundaries.[25]

The STM design described in this article allows for easy *in situ* manipulation of the STM tip. The dumbbell tip assembly is pulled against two metal rails by a SmCo magnet, and thus is only held by friction on the metal rails. This dumbbell can easily be removed from the piezo tube by using tweezers attached to the end of the pincer jaw of a wobble stick. Once removed, the dumbbell can be put into a storage location or transferred to the tip heater and sputtering device. The assembly is shown in Fig. 6. For heating and/or sputtering, the dumbbell containing the tip is put into a hole in the molybdenum block of the heating/sputtering device so that only the end of the tip extends out from the block. The mount is spring-loaded to ensure good electrical contact between the dumbbell and molybdenum block. Next, the whole molybdenum block is pushed on a stainless-steel tray with the wobble stick until the tip position is underneath the filament. The distance between tip and filament is about 2–3 mm. For electron-beam heating, the tip and tray in contact with the molybdenum block are biased positively to about 700 V. The filament is enclosed in a cylindrical Ta shield that may be biased negatively during electron-beam heating of the tip. The Mo block and stainless-steel tray, which are both at high voltage, are shielded from electrons by a metal cover connected to one of the filament posts. This shield is at the same low potential as the filament. A thermocouple that was attached to a tip for test purposes showed that temperatures above 2000 K can be achieved readily. However, the actual temperature at the very end of the tip cannot be reliably estimated from a thermocouple reading. Scanning electron microscopy images of tungsten tips heated with this setup showed that an electron emission current from the filament

of 15 mA at a bias of 700 V (10.5 W) was sufficient to melt the very end of the tungsten tips.

Alternatively, the tip can be cleaned by ion sputtering. Ions are generated by backfilling the UHV chamber with argon to a pressure of 5×10^{-5} Torr, heating the filament to achieve thermionic emission, and then biasing the Ta shield positively to about 200 V. Ions are then accelerated toward the tip by applying a negative bias of -500 V. These parameters resulted in an ion current of 0.5 μA measured at the tip.

After cleaning, the tip can be placed back in the STM head by simply reversing the transfer routine procedure.

III. PERFORMANCE

The STM described here has been used to image various metallic and bimetallic surfaces,[28,29] as well as oxidized Sn/Pt surface alloys.[30–32] Standard cleaning procedures utilizing ion bombardment and annealing in O_2 were used to prepare the samples for atomic resolution imaging using STM. To prepare the SnPt surface alloys, we evaporated submonolayer amounts of Sn (6N ingot) from a resistively heated Ta ''boat'' onto the sample. The desorption rate was established with Sn uptake plots produced by using AES. Annealing of the sample results in different ordered alloys depending on the initial Sn coverage and annealing temperature. The chamber base pressure was typically 2×10^{-10} Torr, and the pressure did not exceed 2×10^{-9} Torr during metal dosing.

The STM tips were electrochemically etched from 0.015- in. polycrystalline tungsten wire in a 2 M NaOH solution. They were then dipped in HF for 15–20 s to remove much of the oxide layer and any contamination that may have been deposited during etching.[33] This procedure has resulted in high quality tips that often require no further *in situ* cleaning. During an experiment, tip conditioning is done using voltage pulses, controlled contact with the sample, and, in some cases, field emission. Our tip treatment stage also houses several extra tips in dumbbells that can be used if necessary.

Typical ''large-area'' scans using this setup rarely exceeded 200 nm. Scanning rates depended on the surface topography and area. For small scans (50×50 Å), rates as high as 8 ms/line were used. Scan rates for most images varied between 30–300 ms/line. The intrinsic resonance frequency for this STM was not measured.

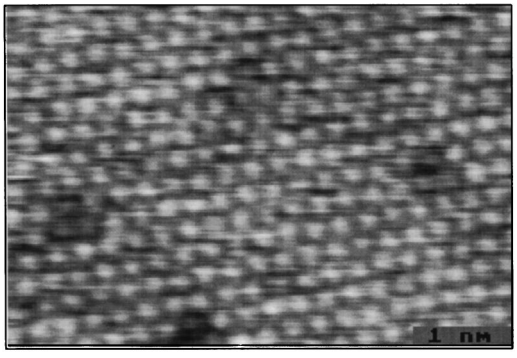

FIG. 7. Atomic resolution image of Pt(111). Image size is 5.4×4.2 nm ($V_t=-4.46$, $I=0.22$ nA).

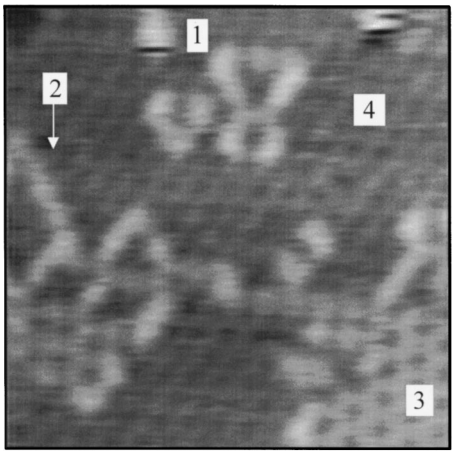

FIG. 8. Sn/Pt(111) surface alloy showing (1) defect sites, (2) antiphase boundary, (3) ordered (2×2) region, and (4) ordered ($\sqrt{3}\times\sqrt{3}$)R30° domain. Image size is 7.5×7.6 nm ($V_t=-276$ mV, $I=0.46$ nA).

In our first efforts with this STM, we imaged the Pt(111) single crystal surface with atomic resolution as shown in Fig. 7. We used these early images to calibrate the piezo deflection using the interatomic spacing (2.77 Å) of Pt(111) as a reference.

Figure 8 shows an image of a mixed domain region from a Sn/Pt(111) surface alloy.[28] In this experiment, we were able to observe chemical contrast, imaging alloyed Sn in the surface layer as depressions. Although Sn is known to be physically buckled out from the surface plane by 0.022 ± 0.005 nm according to ion scattering results,[34] Sn atoms are imaged as *depressions*. This is due to a lower density-of-states for Sn at the Fermi level than for Pt when alloyed as calculated by Pick.[35] More significantly, the measured corrugation for the (2×2) and ($\sqrt{3}\times\sqrt{3}$)R30° regions and domain boundaries differs depending on the number of nearest-neighbor-Sn atoms around a Pt atom, exhibiting *electronic contrast*. This result illustrates the importance of ''ligand'' effects on the chemical properties of Sn/Pt(111) alloys, which had previously been attributed primarily to site blocking or ''ensemble'' effects.

One of the main advantages of the design of this instrument is the ease of switching between analytical techniques. We were able to perform analyses using several surface-science techniques on a sample under specific, identical con-

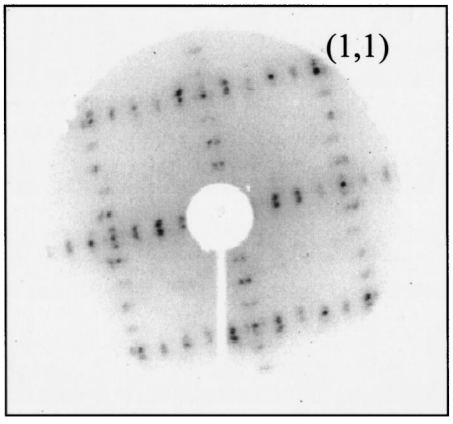

FIG. 9. LEED image at $E_p=56$ eV of the reconstructed Pt(100) surface showing a 5×20 structure.

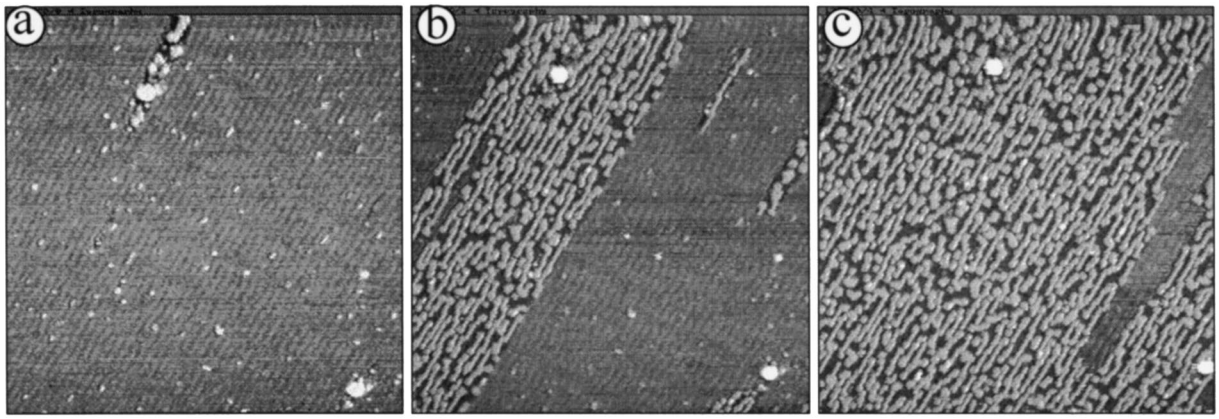

FIG. 10. Reconstructed Pt(100)-hex surface (a) prior to, (b) during, and (c) following CO adsorption. Total time was 30 min. Image size is 60.5×60.5 nm. Tunneling conditions for all images were $V_t = -400$ mV, $I = 0.12$ nA.

ditions. This eliminates inconsistencies that may arise from running parallel experiments or transferring samples. A typical experiment involving the CO-induced lifting of the Pt(100)-hex 0.7° reconstruction was performed in our chamber which can be illustrated by several figures. AES and LEED were used to verify that the surface was clean and had long-range order. Figure 9 shows a LEED pattern characteristic of the Pt(100)-hex reconstruction. STM was used to observe the local structure of the surface in ''snap shots,'' i.e., sequential imaging of the adsorbate-induced lifting of the hex reconstruction. The chamber was pressurized to 1×10^{-8}-Torr CO and a series of images were taken. As one can see in Fig. 10, the clean Pt(100)-hex surface reconstruction was disrupted quickly and completely eliminated after 30 min. A small-scale image of the final state of the CO-covered Pt islands, which exhibit a $c(2\times2)$ structure, is shown in Fig. 11.

These results demonstrate the utility of our UHV system for performing through surface characterization studies. By incorporating several traditional surface-analytical instruments into a single chamber, we eliminate inconsistencies in sample condition due to *ex situ* sample transfer and/or the necessity to run parallel experiments. With the inclusion of FT-IRAS, this system is capable of a broad range of experiments on chemical reactions at surfaces.

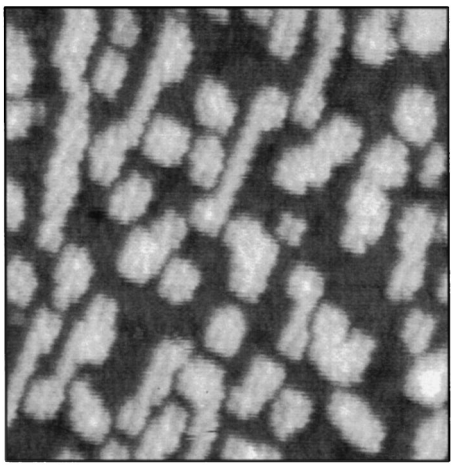

FIG. 11. Unreconstructed Pt(100) surface with adsorbed $c(2\times2)$-CO layer. Image size is 16.6×16 nm ($V_t = -95$ mV, $I = 0.18$ nA).

ACKNOWLEDGMENTS

This work was partially supported by the Analytical and Surface Chemistry Program in the Division of Chemistry, National Science Foundation (NSF).

[1] G. Binnig and H. Rohrer, Helv. Phys. Acta **55**, 726 (1982).
[2] G. Binnig, H. Rohrer, C. Gerber, and E. Weibel, Phys. Rev. Lett. **49**, 57 (1982).
[3] L. J. Lauhon and W. Ho, Phys. Rev. B **60**, R8525 (1999).
[4] M. A. Rezaei, B. C. Stipe, and W. Ho, J. Chem. Phys. **109**, 6075 (1998).
[5] M. T. Paffett, A. D. Logan, R. J. Simonson, and B. E. Koel, Surf. Sci. **250**, 123 (1991).
[6] M. T. Paffett and R. G. Windham, Surf. Sci. **208**, 34 (1989).
[7] Y. Li and B. E. Koel, Surf. Sci. **330**, 193 (1995).
[8] M. T. Paffett, S. C. Gebhard, R. G. Windham, and B. E. Koel, J. Phys. Chem. **94**, 6831 (1990).
[9] C. Xu and B. E. Koel, Surf. Sci. **310**, 198 (1994).
[10] C. Xu and B. E. Koel, Surf. Sci. **304**, L505 (1994).
[11] M. R. Peng and J. E. Reutt-Robey, Surf. Sci. **336**, L755 (1995).
[12] E. P. Go, K. Thuermer, and J. E. Reutt-Robey, Surf. Sci. **437**, 377 (1999).
[13] S. L. Silva, T. M. Pham, A. A. Patel, S. Haq, and F. M. Leibsle, Surf. Sci. **452**, 79 (2000).
[14] K. Namba, T. Komeda, and Y. Nishioka, Surf. Sci. **117/118**, 189 (1997).
[15] M. Bott, T. Michely, and G. Comsa, Rev. Sci. Instrum. **66**, 4135 (1995).
[16] S. Horch, P. Zeppenfeld, R. David, and G. Comsa, Rev. Sci. Instrum. **65**, 3204 (1994).
[17] U. Dürig (personal communication).
[18] W. Crew and R. J. Madix, Rev. Sci. Instrum. **66**, 4552 (1995).
[19] F. Mugele, C. Kloos, and P. Leiderer, Rev. Sci. Instrum. **67**, 2557 (1996).
[20] F. Mugele, A. Rettenberger, J. Boneberg, and P. Leiderer, Rev. Sci. Instrum. **69**, 1765 (1998).
[21] V. T. Binh, J. Microsc. **152**, 355 (1988).
[22] V. T. Binh and J. Marien, Surf. Sci. **202**, L539 (1988).
[23] I. Ekvall, E. Wahlstrom, D. Claesson, H. Olin, and E. Olsson, Meas. Sci. Technol. **10**, 11 (1999).
[24] O. Albreksten, H. W. M. Salemink, K. A. Morch, and A. R. Tholen, J. Vac. Sci. Technol. B **12**, 3187 (1994).
[25] D. K. Biegelsen, F. A. Ponce, J. C. Tramontana, and S. M. Koch, Appl. Phys. Lett. **50**, 696 (1987).
[26] D. K. Biegelsen, F. A. Ponce, J. C. Tramontana, and S. M. Koch, Appl. Phys. Lett. **54**, 1223 (1989).
[27] S. Morishita and F. Okuyama, J. Vac. Sci. Technol. A **9**, 167 (1991).
[28] M. Batzill, D. E. Beck, and B. E. Koel, Surf. Sci. **466**, L821 (2000).
[29] D. E. Beck, M. Batzill, and B. E. Koel (submitted).
[30] M. Batzill, D. E. Beck, and B. E. Koel, Appl. Phys. Lett. **78**, 2766 (2001).
[31] M. Batzill, D. E. Beck, and B. E. Koel, J. Vac. Sci. Technol. (in press).
[32] M. Batzill, D. E. Beck, and B. E. Koel, Phys. Rev. B **64**, 5402 (2001).
[33] L. A. Hockett and S. E. Creager, Rev. Sci. Instrum. **64**, 263 (1992).
[34] S. H. Overbury, D. R. Mullins, M. T. Paffett, and B. E. Koel, Surf. Sci. **254**, 45 (1991).
[35] S. Pick, Surf. Sci. **436**, 220 (1999).